行政院國家科學委員會專題研究計畫　期中進度報告

奈米結構沉積製程與積體電路製程之整合

計畫類別：整合型計畫
計畫編號：NSC93-2120-M-009-007-
執行期間：93 年 08 月 01 日至 94 年 07 月 31 日
執行單位：國立交通大學材料科學工程研究所

計畫主持人：潘扶民

計畫參與人員：林貞君，陳柏林，陳德銘，張凱鈞

報告類型：精簡報告
報告附件：出席國際會議研究心得報告及發表論文
處理方式：本計畫可公開查詢

中　華　民　國 94 年 5 月 23 日

行政院國家科學委員會專題研究計畫成果報告

奈米解析度記錄媒體及其他應用之包覆合金碳奈米結構陣列，其製造、機械/熱性質及製程特徵之研究

子計畫三(2/3)-奈米結構沉積製程與積體電路製程之整合

計畫編號：93-2120-M-009-007-

執行期限：93 年 08 月 01 日至 94 年 07 月 31 日

主持人：潘扶民　國立交通大學材料科學與工程研究所

共同主持人：

計畫參與人員：林貞君，陳柏林，陳德銘，張凱鈞

中文摘要

我們本計畫的第二年度內的主要研究內容為：(1) 以製作陽極氧化鋁(anodic aluminum oxide, AAO)自組裝奈米孔洞陣列結構做為版模，在矽基材製作 TiO_2 奈米點三極體結構；(2)以 AAO 奈米孔洞陣列結構做為版模開發奈米碳管(carbon nanotube, CNT) 選區成長與控制碳管濃度製程技術。利用奈米點作為電子發射源製作場效發射三極體元件，此場效發射三極體擁有 45 伏特之低閘極啟始電壓，且在 120 伏特的閘極電壓下，場效發射電流密度高達 25 毫安培/平方公分。此奈米點之電子發射源具有低製成溫度與極佳的均勻性等優點，將可滿足大面積場效發射顯示器之製程需求。奈米碳管的成長受到奈米孔洞的限制與外加偏壓或電漿自我偏壓的影響，因此具有極佳的垂直準直性。藉由調整甲烷與氫氣之反應氣體比例即可有效地控制奈米碳管成長出奈米孔洞外之管束密度。

關鍵詞：陽極氧化鋁、碳奈米管、場效發射三極體、啟始電壓

Abstract

We have carried out two research tasks in the second project year: (1) fabrication of triode-type field emission structure using the titanium oxide nanodot arrays on silicon substrate using the AAO as the template; (2) tunable tube density of CNTs grown from the AAO nanopores. A field emission triode device using the self-organized nanodot arrays as electron emission source was proposed and fabricated. The field emission triodes exhibited a low gate turn-on voltage of 45 V and high emission current density of 25 mA/cm^2 at 120 V. The desirable electric properties and easily controllable fabrication process of the nanodot triodes show potential for application in field emission displays and vacuum microelectronics. Ordered arrays of CNTs were prepared by using the AAO films as templates and the segments of CNTs stretching out of the AAO nanopores still maintain relatively good alignment. We have also demonstrated that the tube number density of aligned CNTs grown over the AAO template can be directly controlled by adjusting the CH_4/H_2 feed ratio during the CNT growth.

Keywords

anodic aluminum oxide (AAO), carbon nanotube (CNT), field emission triode, turn-on voltage

1. Introduction

Cold-cathode field emitter arrays (FEAs) have been the subject of intense research, primarily because of potential applications for many technologies, such as field emission flat panel displays, cold-cathode microwave devices, and electron guns in the x-ray tubes. For practical applications, FEAs must have a low turn-on voltage, high emission current density, high current stability, and a long lifetime. In the past decade, numerous nanostructured materials, including carbon nanotubes (CNTs),[1-3] carbon nanoparticles (CNPs),[4] IrO_2

nanorods,[5] ZnO nanowires,[6,7] MoS_2 nanoflowers,[8] etc., have been extensively studied to achieve the goal.

In our previous studies, we used nanoporous anodic aluminum oxide (AAO) films as the mask for local anodic oxidation of metal films to fabricate nanodot arrays of metal oxides.[9,10] By using the AAO mask as the anodization template for metallic thin films, one can produce ordered arrays of oxide nanodots with a very high packing density (as high as 10^{10} cm^{-2}) and a uniform size distribution. In addition, the thus fabricated nanodots of metal oxides provide stable chemical and microstructure properties, whereas metallic FEAs (e.g., molybdenum and niobium tips) have shown increasing tendency to oxidation under normal operation conditions, resulting in emission current fluctuation.[11,12] Tatarenko *et al.*[13] have demonstrated that oxide nanodots with a high geometrical enhancement have a high field emission efficiency. In order to study the feasibility of integration of the nanodot arrays into conventional integrated circuit (IC) process technology for field emission applications, we have fabricated the triode-type field emission structure using the titanium oxide nanodot arrays as the cold cathode.

The second part of our work is to use CNTs as another field electron emitter material. For field mission display application, it is necessary to grow vertically aligned CNT arrays on a large area with suitable tube density and tube dimensions. In recent years, template methods, such as AAO nanotemplates in particular, have been widely introduced to produce well aligned and monodispersed CNT arrays.[14] We report that the tube density of the cobalt-catalyzed CNTs on the AAO template can be controlled by regulating the flow rate ratio of methane (CH_4) to hydrogen (H_2) precursor gases during the CNT growth, and thereby field emission characteristics of CNTs can be adjusted.

2. Experimental

(1) Triode-type field emission structure using the titanium oxide nanodot arrays

Figure 1 illustrates the fabrication process of nanodot-based field emission triodes. Figs. 1a-1c show the preparation steps of the nanodot emitter, and Figs. 1d-1i show the fabrication steps of the triode structure. At first, as-deposited Al/Ti film stack are oxidized by electrochemical anodization. The AAO templated nanodots have an average diameter of about 40 nm and an average height of about 30 nm and then annealed at 450^{o}C in a high vacuum furnace for 2 hour. A dielectric layer of tetraethoxysilane (TEOS) oxide layer and a titanium layer were directly deposited onto the nanodot array respectively. The gate aperture array with a diameter of 20 μm was defined on the titanium layer with a photolithography system and etched by Reactive ion etching (RIE). After the RIE, the sample was dipped into a dilute HF solution for a few seconds to sweep away the residual TEOS oxide on nanodots in the triodes. In the final step, the photoresist was removed by acetone (Fig. 1i) and fabrication of the nanodot triodes was completed. The field emission properties of the triode devices were characterized by electrical microprobes equipped in a FE-SEM system with a base pressure of 10^{-7} Torr.

(2) Tunable tube density of CNTs grown from the AAO nanopores

Ordered AAO pore channel arrays were prepared by two-step anodization and the Co catalyst for the CNT growth was electrochemically deposited at the pore bottom. The CNT growth was carried out in the electron cyclotron resonance chemical deposition (ECR-CVD) system. The gas mixture of CH_4 and H_2 was used as the carbon source carbon source and the total gas flow rate was kept constant at 22 sccm. The CH_4 concentration in the gas precursor was varied from 9% to 91% in order to investigate the influence of the CH_4/H_2 ratio on the CNT growth.

The field emission measurements were conducted by the simple diode configuration and performed in a vacuum about 10^{-6} Torr. The anode is a platinum wire with a hemispherical tip 1 mm in diameter. The distance between the CNTs and the anode

was about 100 μm.

3. Results and Discussion

(1) Triode-type field emission structure using the titanium oxide nanodot arrays

In order to study the feasibility of integration of the nanodot arrays into conventional integrated circuit (IC) process technology for field emission applications, we have fabricated the triode-type field emission structure using the titanium oxide nanodot arrays as the cold cathode. A side-view SEM image of the triode arrays is shown in Figure 2a. The triode sample contains 16×16 arrays of gated cathode cells. Fig. 2b shows a higher magnification image of the nanodot emitter arrays inside the gate aperture. The SEM image clearly shows that the titanium oxide nanodot arrays maintain their geometrical configuration without discernable damage after the dilute HF dip and the RIE processes. This demonstrates the feasibility of fabrication of nanodot-based field emission devices using standard microfabrication techniques. The microprobes can be manipulated by piezo-driven linear nanomotors with a minimum step size of 10 nm in the *x*-*y*-*z* directions. Figure 3 is the *in situ* SEM image showing the configuration of field emission measurement for a triode using tungsten microprobes. The cathode (nanodot emitters) was grounded and the gate electrode was connected to the microprobe with the positive bias sweeping from 0 to 120 V. The field emitted electrons were collected by a microprobe (anode), which was about 10 μm away from the gate aperture and biased with +50 V. Since the triode cells were well separated, this measurement configuration allowed us to measure the field emission properties of individual gated cathode cells by the microprobes. The supply of the dc bias and field emission measurement were performed with high voltage source-measurement units (Keithley 237). Figure 4 shows the gate-voltage dependence of the emission current of the nanodot triodes. The electron emission started at the gate voltage of about 45 V, and the anode current exceeded 80 nA when the gate voltage was increased to 120 V. Because the measured anode current was mainly provided by one single cathode cell (gate aperture) under the anode probe, the anode current of 80 nA measured at a gate voltage of 120 V corresponds to an emission current density of 25 mA/cm^2 (one aperture area ~ 3×10^{-6} cm^2). As compared the field emission result of the cathode cells with one another, little difference was observed, suggesting an excellent distribution uniformity of nanodot emitters in the triodes. The F-N plot of the anode current shown in the inset of Fig. 4 also exhibits a linear F-N fit, confirming that the field emitted electrons extracted by the gate bias was responsible for the measured anode current. Although the titanium oxide nanodots in the triodes show satisfactory field emission characteristics, the current leakage from the emitters to the gate electrodes was large. The measured gate current is about 50% of the anode current as shown in Fig. 4. The detection of the high gate current is owing to that the whole 16×16 arrays of gated cathode cells are biased by the same gate electrode, and leakage currents of all the cathode cells were, therefore, measured simultaneously. In contrast, the anode current was practically measured from only one cathode cell.

(2) Tunable tube density of CNTs grown from the AAO nanopores

Figures 5(a)–5(c) show the side-view SEM of the AAO templated CNTs grown at CH_4 concentrations of 9%, 50%, and 91%, respectively. At the CH_4 concentration of 9% (see Fig. 5(a)), the tube density of CNT is as high as 9.0×10^9 tubes/cm^2, indicating a pore-filling ratio of about 82%, which is defined as the density ratio of the nanotubes to the AAO pores. At an extremely high CH_4 concentration of 91% (see Fig. 5(c)), the tube density decreases significantly to about 2.0×10^9 tubes/cm^2, corresponding to a pore-filling ratio of about 18%. The inset in Fig. 5(b) shows the transmission electron microscopy (TEM) image of the CNTs. It

clearly shows that a Co catalyst particle is encapsulated at the tube tip and covered by graphitic cap, suggesting that the CNT growth is via the tip-growth mechanism.[15] During the CNT growth in the CH_4/H_2 plasma, the *a*-C by-product is concurrently deposited on the AAO template, and the *a*-C deposition seems to play an important role in control of the tube density of CNTs on the AAO template whereas it can be quickly etched away by reactive hydrogen species in the plasma.[16] At a high CH_4/H_2 feed ratio, the *a*-C deposition overwhelms the etch reaction, resulting in steady growth of the *a*-C.[17] The *a*-C layer will gradually cover up the AAO nanopores and prevent nanotubes from growing out of the nanopores. As shown in the inset of Fig. 5(c), some short nanotubes marked by white arrows are buried inside the nanopores. Those CNTs which have already grown out of the nanopores can continuously grow up since the CNT growing site is at the tip of the nanotubes stip-growth mechanismd. At the CH_4 concentration of 91%, only about 18% of CNTs grew out of the AAO nanopores. On the other hand, at a low CH_4/H_2 feed ratio, the AAO surface is almost free from the *a*-C layer (see the inset of Fig. 5(a)) since it was quickly etched away by hydrogen species, leading to efficient CNT growth and thus a very high tube density. Figure 5(d) shows that the tube density is inversely proportional to the CH_4 concentration. In addition to the tube density, the CNTs grown at CH_4 concentration of 91% are shorter than those grown at 50% and 9% as shown in Figs. 5(a)-(c). This is probably due to that the *a*-C layer may also be deposited on the CNT, which can hinder reactive carbonaceous species from reaching the Co catalyst, hence reducing the CNT growth rate.

4. Conclusions

In summary, field emitter arrays of titanium oxide nanodots were prepared on the silicon wafer by electrochemical anodization of the titanium thin film in terms of AAO templation. Fabrication of the field emission triodes is compatible with conventional IC technology. Field emission properties of individual gated cathode cells have been studied using electrical microprobes in an FE-SEM system, and a low gate turn-on voltage of 45 V and considerably high emission current density of 25 mA/cm^2 at 120 V were measured.
The tube number density of aligned CNTs grown over the nanoporous AAO template can be directly controlled by adjusting the CH_4/H_2 feed ratio during the CNT growth. A high CH_4 concentration leads to the heavy deposition of an *a*-C deposit on the AAO surface. Although the *a*-C can effectively decrease the CNT density on the AAO template, thereby decreasing the field-screening effect and increasing the field enhancement, it notably deteriorates the electron field emission property of the CNTs. The nonlinearity of the F–N plot of the CNTs is ascribed to the deposition of the *a*-C overlayer on the CNT tip. The CNTs grown at 50% CH_4 show the best field emission property.

References

1. Walt A. de Heer, A. Châtelain, and D. Ugarte, Science, **270**, 1179 (1995).
2. Yahachi Saito and Sashiro Uemura, Carbon, **38**, 169 (2000).
3. Jean-Marc Bonard, Jean-Paul Salvetat, Thomas Stöckli, Walt A. de Heer, László Forró, and André Châtelain, Appl. Phys. Lett., **73**, 918 (1998).
4. Kyung Ho Park, Hyung Jun Han, Seungho Choi, Kyung Moon Lee, Soonil Lee, and Ken Ha Koh, J. Vac. Sci. Technol. B, **21**, 562 (2003).
5. Reui-San Chen, Ying-Sheng Huang, Ya-Min Liang, Chim-Sung Hsieh, Dah-Shyang Tsai, and Kwong-Kau Tiong, Appl. Phys. Lett., **84**, 1552 (2004).
6. Yung-Kuan Tseng, Chorng-Jye Huang, Hsin-Min Chen, I-Nan Lin, Kuo-Shung Liu, and I-Cherng, Adv. Funct. Mater., **13**, 811 (2003).
7. S. H. Jo, J. Y. Lao, Z. F. Ren, R. A. Farrer, T. Baldacchini, and J. T. Fourkas, Appl. Phys. Lett., **83**, 4821 (2003).

8. Y. B. Li, Y. Bando, and D. Golberg, Appl. Phys. Lett., **82**, 1962 (2003).
9. Po-Lin Chen, Cheng-Tzu Kuo, Tzeng-Guang Tsai, Bo-Wei Wu, Chiung-Chih Hsu, and Fu-Ming Pan, Appl. Phys. Lett., **82**, 2796 (2003).
10. Po-Lin Chen, Cheng-Tzu Kuo, Fu-Ming Pan, and Tzeng-Guang Tsai, Appl. Phys. Lett., **84**, 3888 (2004).
11. S. Itoh, T. Niiyama, and M. Ykoyama, J. Vac. Sci. Technol. B, **11**, 647 (1993).
12. B. R. Chalamala, R. M. Wallace, and B. E. Gnade, J. Vac. Sci. Technol. B, **16**, 2859 (1998).
13. N. I. Tatarenko, V. A. Solntsev, and A. N. Rodionov, J. Vac. Sci. Technol. B, **17**, 647 (1999).
14. J. Li, C. Papadopoulos, J. M. Xu, and M. Moskovits, Appl. Phys. Lett. **75**, 367 (1999).
15. R. T. K. Baker, Carbon **27**, 315 (1989).
16. Olivier M. Küttel, Oliver Groening, Christoph Emmenegger, and Louis Schlapbach, Appl. Phys. Lett. **73**, 2113 (1998).
17. K. B. K. Teo, M. Chhowalla, G. A. J. Amaratunga, W. I. Milne, G. Pirio, P. Legagneux, F. Wyczisk, J. Olivier, and D. Pribat, J. Vac. Sci. Technol. B **20**, 116 (2002).
.

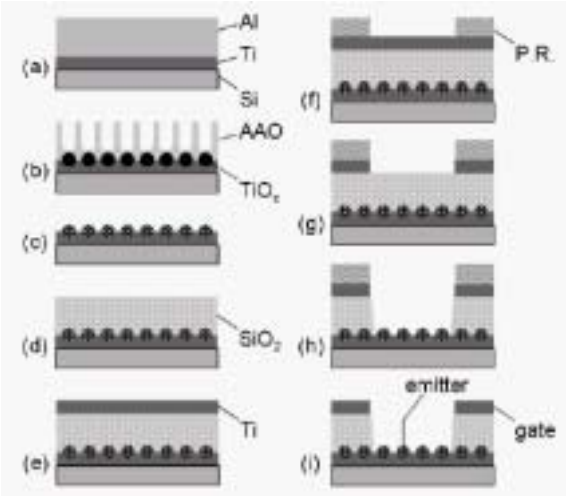

Figure 1. Fabrication steps for the TiO_2 nanodot-based field emission triodes. (a) Ti and Al deposition, (b) anodization, (c) AAO removal and vacuum annealing, (d) TEOS oxide deposition, (e) Ti deposition, (f) photoresist pattern formation, (g) dry etching of Ti, (h) dry etching of TEOS oxide, and (i) lift-off the photoresist.

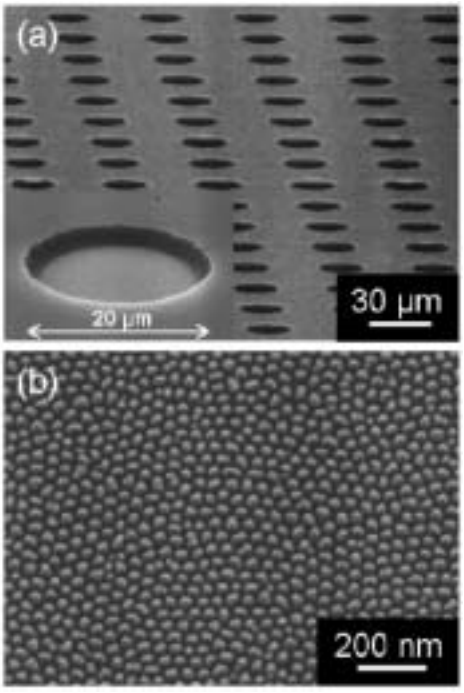

Figure 2. (a) Side-view FE-SEM image of the nanodot-based field emission triode array. The inset shows the enlarged image of a triode. (b) Side-view FE-SEM image of the TiO_2 nanodot emitters in the triode.

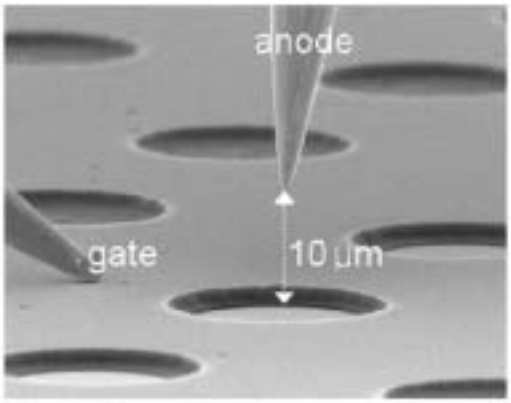

Figure 3. FE-SEM image of the field emission measurement configuration for a triode device. The tip of anode microprobe is about 10 μm away from the gate electrode.

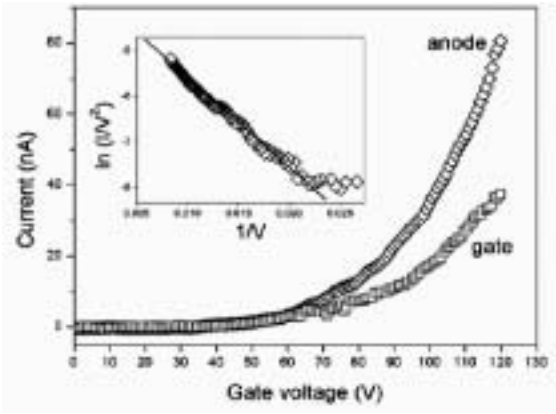

Figure 4. Gate-voltage dependence of the anode and gate current of the triode. The inset shows the corresponding Fowler-Nordheim plot of the anode current.

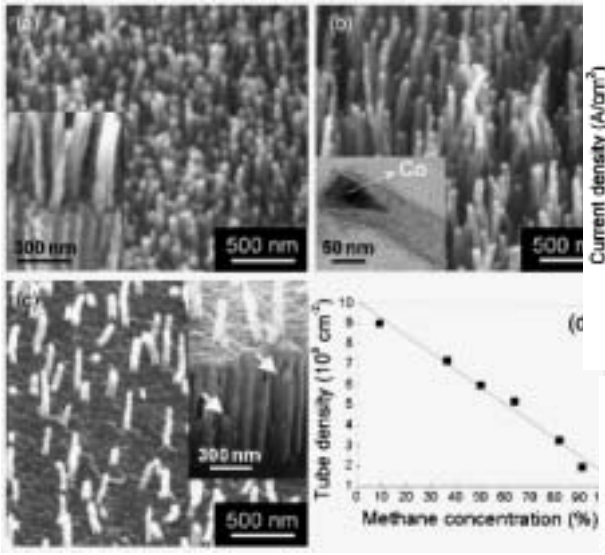

Figure 5. Side-view SEM images of the AAO templated CNTs grown at CH_4 concentrations of (a) 9%, (b) 50%, and (c) 91%. The insets in (a) and (c) are the cross-sectional view of the CNTs. The inset in (b) is the TEM image of the CNT. (d) The tube density of CNTs grown over the AAO nanopores as a function of the CH_4 concentration.

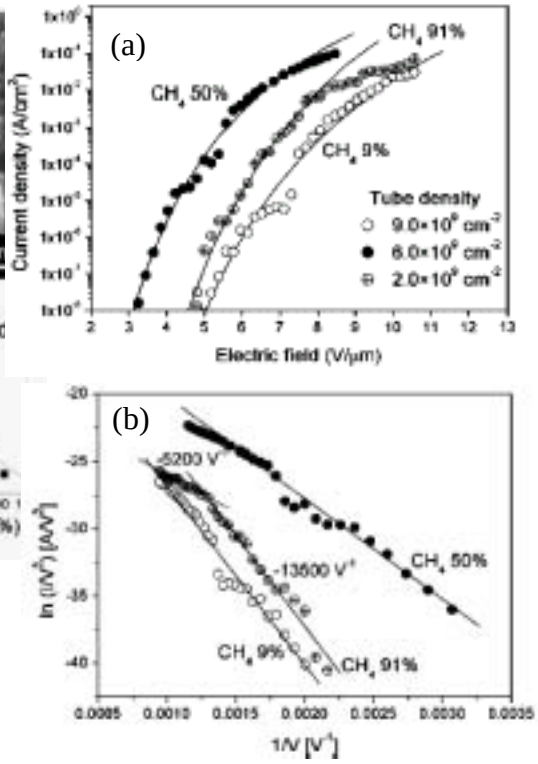

Figure 6. (a) Field emission current density (J) as a function of electric field (E) for the CNTs grown on the AAO template with the three different tube densities shown in Figs. 5(a)–(c). The solid curves are F–N fits using the low current/field regions which do not show saturation. (b) Corresponding F–N plots of data. The slopes of the F–N plot for the CNTs grown at 91% CH_4 are also indicated in the figure.